

# Enhancement of basal plane electrocatalytic hydrogen evolution activity via joint utilization of trivial and non-trivial surface states

Qun Yang<sup>a</sup>, Congcong Le<sup>a</sup>, Guowei Li<sup>a</sup>, Thomas Heine<sup>b,\*</sup>, Claudia Felser<sup>a,\*</sup>, Yan Sun<sup>a,\*</sup>

<sup>a</sup> Max Planck Institute for Chemical Physics of Solids, 01187 Dresden, Germany

<sup>b</sup> Faculty of Chemistry and Food Chemistry, Technische Universität Dresden, 01069 Dresden, Germany

## ARTICLE INFO

### Article history:

Received 9 October 2020

Revised 7 December 2020

Accepted 20 December 2020

### Keywords:

Density functional theory  
Hydrogen evolution reaction  
Topological semimetal  
Dangling-bonds  
Topological surface states  
Gibbs free energy

## ABSTRACT

Transition metal dichalcogenide semiconductors, particularly MoS<sub>2</sub>, are known as promising alternative non-precious hydrogen evolution reaction (HER) electrocatalysts to high-cost Pt. However, their performance is strongly limited by the poor conductivity and lack of active sites in the basal plane. Therefore, it is desirable to find alternatives with active basal plane sites or develop facile strategies to optimize the inert basal plane. In this work, we study the HER over topological semimetal Nb<sub>2</sub>S<sub>2</sub>C based on its basal plane. We report the first successful activation and optimization of the basal plane of Nb<sub>2</sub>S<sub>2</sub>C by synergistic using trivial surface states (SSs) and nontrivial topological surface states (TSSs). We find that the binding strength towards hydrogen adsorption of the easily cleaved sulfur(S)-terminated Nb<sub>2</sub>S<sub>2</sub>C surface can be stronger than that of 2H-MoS<sub>2</sub>, attributing to the presence of trivial SSs and nontrivial TSSs in Nb<sub>2</sub>S<sub>2</sub>C. By creating S vacancy on the basal plane, the binding strength towards hydrogen adsorption can be greatly optimized. The TSSs together with dangling-bonds reduce the Gibbs free energy to 0.31 eV, close to the peak of the volcano plot. This study provides a promising strategy for the joint utilization of the basal plane trivial SSs and TSSs for the HER.

© 2021 The Authors. Published by Elsevier Ltd.  
This is an open access article under the CC BY license (<http://creativecommons.org/licenses/by/4.0/>)

## 1. Introduction

H<sub>2</sub> is one of the most important next-generation energy carrier candidates owing to its high-energy density and environmental friendliness. Electrochemical water splitting has been considered one of the most effective ways for H<sub>2</sub> production. Moreover, it has been established that the catalytic activity of transition metal surfaces follows well-defined volcano plots, and precious-metal-based materials, such as Pt and Pt-based materials, present the most favorable Gibbs free energy ( $\Delta G_{H^*}$ ) for hydrogen (H) binding [1–3]. However, the scarcity and high-cost of precious metals greatly limit their practical applications. Because of the natural characteristics of active, earth-abundant, and inexpensive, layered materials, such as MoS<sub>2</sub>, they have been considered as promising electrocatalyst alternatives to precious metals [4–9]. However, most layered materials present shortcomings. For example, semiconducting 2H-MoS<sub>2</sub>, the most stable phase, shows poor electrical conductivity, which

hinders the charge-transfer kinetics. In addition, its surface sulfur (S) atoms are chemically saturated which leads to weak interactions with H. It was confirmed that the chemically active sites originate only from the metallic edges, and the large surface area is catalytically inert [10,11]. Various techniques, such as phase engineering [12,13], defect engineering [14–18], strain engineering [19], and chemical doping [20,21] have been developed to overcome this limitation and activate the inert basal plane of MoS<sub>2</sub>.

Recently, it was demonstrated that the metallic topological surface states (TSSs) near the Fermi level were effective for facilitating the charge-transfer kinetics during various heterogeneous catalysis reactions [22,23]. Some topological materials were suggested as promising catalysts, for example, Weyl semimetals (Nb, Ta)/(As, P) and MoTe<sub>2</sub> as HER photocatalysts [24], Bi<sub>2</sub>Se<sub>3</sub>/ZnSe heterostructures [25], Weyl semimetal Co<sub>3</sub>Sn<sub>2</sub>S [26], Pt-based multi-fold fermion semimetals [27], and nodal-line semimetal TiSi [28], et al., as HER electrocatalysts. Moreover, the catalytic properties of some topological semimetals were experimentally verified [24,26,27,29]. Among the experimentally tested excellent topological catalysts, we find that topological semimetals have their natural advantage over fully gapped topological insulators, and that can be attributed to the synergistic effect of the metallic bulk states and

\* Corresponding authors.

E-mail addresses: Thomas.Heine@tu-dresden.de (T. Heine),  
Claudia.Felser@cpfs.mpg.de (C. Felser), Yan.Sun@cpfs.mpg.de (Y. Sun).

robust TSSs. These promising topological catalytic materials inspire us to optimize the inert basal plane of topological semimetals using the TSSs.

In this study, we make a pioneering exploration of the importance of surface states (SSs) for basal plane HER performance. We find that unlike the binding strength for H adsorption on the inert basal plane of 2H-MoS<sub>2</sub>, the topological semimetal Nb<sub>2</sub>S<sub>2</sub>C basal plane can be improved via the synergistic effect of the S-3p<sub>z</sub>-orbital-based trivial SSs and S-3p<sub>x</sub> and S-3p<sub>y</sub>-orbital-based non-trivial TSSs, but only to a certain extent, due to the limited S-3p<sub>z</sub> SSs in the pristine Nb<sub>2</sub>S<sub>2</sub>C basal plane. The defective Nb<sub>2</sub>S<sub>2</sub>C basal plane with Nb-4d<sub>z<sup>2</sup></sub>-orbital-dominated TSSs can directly interact with H adsorbate. Besides, the defective Nb<sub>2</sub>S<sub>2</sub>C presents more Nb-4d<sub>xz</sub> and Nb-4d<sub>x<sup>2</sup>-y<sup>2</sup></sub>-orbital-based trivial SSs. Owing to the suitable orbital orientation, they can also provide favourable charge interaction with adsorbed H. Those chemically active orbitals enable energetically and sterically favourable hydrogen adsorption/desorption. Hence, the synergism of the trivial dangling-bonds and TSSs contribute to the greatly optimized  $\Delta G_{H^*}$  (where the \* denotes an active site on the surface and  $H^*$  is the reaction intermediate) of 0.31 eV for H adsorption. This study enriches our understanding of the joint effect from dangling bonds and TSSs in the electrocatalytic process and provides a new strategy for the activation of the inert basal plane of catalysts.

## 2. Computational details

All numerical calculations were performed using the density functional theory (DFT) framework as implemented in the Vienna ab initio simulation package (VASP) [30,31]. The projector augmented wave (PAW) method combined with the Perdew–Burke–Ernzerhof (PBE) generalized gradient approximation were applied [32,33]. The DFT-D3 extension of Grimme was adopted to include the long-range van der Waals (vdW) interactions [34], and Monkhorst–Pack k-point meshes of  $8 \times 8 \times 3$  and  $8 \times 8 \times 1$  were used for bulk and pristine Nb<sub>2</sub>S<sub>2</sub>C slab calculations, respectively. For a surface model, the slab should be thick enough to have a full representation of the surface properties. To confirm the slab thickness, we checked the surface energy dispersion with the increase of the slab thickness (n). As shown in Figure S1, TSSs and trivial SSs present on the slab with  $n = 3$ , and they remain unchanged when further increases the slab thickness. In this work, the easily cleaved (001) basal plane was modeled using a 5 unit-cell-thick slab ( $n = 5$ ) in which the bottom three unit cells were immobilized. To simulate the S-defect, a  $3 \times 3$  slab model with one S vacancy on the basal plane was constructed, and Monkhorst–Pack k-point meshes of  $3 \times 3 \times 1$  and  $6 \times 6 \times 1$  were used for the geometry optimization and electric characteristic calculations. To generate a real space tight-binding model, maximally localized Wannier functions [35] were constructed using the Nb p and d, S p, and C p orbitals. Subsequently, the iterative Green function method was implemented to calculate the SSs of the Nb<sub>2</sub>S<sub>2</sub>C (001) semi-infinite slab [36].

To simulate the H adsorption process, models in which one H adsorbed on the  $1 \times 1$ ,  $2 \times 2$  pristine Nb<sub>2</sub>S<sub>2</sub>C, and  $3 \times 3$  Nb<sub>2</sub>S<sub>2</sub>C with one S-vacancy supercells were constructed, and those corresponded to the H coverages of 1, 1/4, and 1/9, respectively. To predict the HER activity, the Gibbs free energy of the intermediate state,  $\Delta G_{H^*}$ , was calculated using the following equations: [3]

$$\Delta G_{(H^*)} = \Delta E_H + \Delta E_{ZPE} - T \Delta S_H \quad (1)$$

where  $\Delta E_H$  is the H adsorption energy and  $\Delta E_{ZPE}$  and  $\Delta S_H$  are the changes in zero-point energy and entropy between the absorbed H and gaseous H, respectively. According to our calculations,  $\Delta G_{H^*}$  can be obtained as follows:

$$\Delta G_{H^*} = \Delta E_H + 0.27 \text{ eV} \quad (2)$$

## 3. Results and discussion

### 3.1. Geometric structure and topological electronic properties of Nb<sub>2</sub>S<sub>2</sub>C

In 2002, Samaki et al. synthesized 1T-Nb<sub>2</sub>S<sub>2</sub>C for the first time, and determined that it presented trigonal crystal structure with the P $\bar{3}m1$  (164) space group [37]. As illustrated in Figs. 1(a) and (b), Nb<sub>2</sub>S<sub>2</sub>C crystals present a unique layered structure, in which S–Nb–C–Nb–S quintuple layers are linked to one another in AA stacking via vdW forces. For the Nb–C–Nb layers, each [Nb<sub>6</sub>C] octahedron shares six of its twelve edges with adjacent octahedra and the corner Nb atom is shared by three octahedra. The edge linking of [Nb<sub>6</sub>C] octahedra is a common structural feature of transition metal carbides, and the vdW interactions between S layers are a typical structural property of transition metal sulfides. The experimentally measured lattice parameters of Nb<sub>2</sub>S<sub>2</sub>C, which are used for the following calculations, are  $a = b = 3.269 \text{ \AA}$  and  $c = 8.547 \text{ \AA}$  [37].

The band structures of Nb<sub>2</sub>S<sub>2</sub>C without and with spin-orbital coupling (SOC) are depicted in Figs. 1(d) and (e), respectively. In the absence of SOC, band inversion occurs between the Nb-4d<sub>z<sup>2</sup></sub>, S-3p<sub>x</sub>, and S-3p<sub>y</sub> dominated bands near the Fermi level. With the protection of c<sub>3z</sub> rotation symmetry, a Dirac point appears owing to band inversion. Once SOC is included, the Dirac point is broken and the band structure of Nb<sub>2</sub>S<sub>2</sub>C opens a SOC gap at each k-point without band crossings, which enables us to define a Z<sub>2</sub> topological invariant (Fig. 1(e)). By calculating the parities at the time-reversal invariant momenta [38], as shown in Table S1, it is determined that the inverted band gap between bands 19 and 20 form a nontrivial Z<sub>2</sub> index (1;0,0,1) [39–41]. Therefore, TSSs are protected in the inverted band gap. Owing to its layered crystal structure, Nb<sub>2</sub>S<sub>2</sub>C is a good model for the study of the inert basal plane TSSs-related HER. Scheme 1.

### 3.2. Gibbs free energies of Nb<sub>2</sub>S<sub>2</sub>C

After elucidating the topological characteristics of Nb<sub>2</sub>S<sub>2</sub>C, we focus on its HER activity by directly calculating  $\Delta G_{H^*}$ , as illustrated in Fig. 2. Firstly, the natural cleavage plane of S-terminated (001) surface is considered for surface catalytic reactions. As depicted in the inset of Fig. 2, under the H coverage of 1, the most energy favorable H adsorption site is the top of S atom with the  $\Delta G_{H^*}$  calculated to be 1.10 eV. To accurately model the surface HER, especially for the reaction that happens with Volmer–Heyrovsky route, the interfacial solvent effect is also considered to see how it influences the  $\Delta G_{H^*}$  by using the implicit solvent model implemented in VASPsol with a dielectric constant of 80 [42]. We found that the corresponding  $\Delta G_{H^*}$  is 1.083 eV, indicating that solvation effects have a negligible influence on the  $\Delta G_{H^*}$ . Therefore, solvation effect can be ignored in our following calculations. When the H coverage decreased to 1/4, the adsorbed H atom remains at the top of S atom with  $\Delta G_{H^*}$  slightly decreased to 0.86 eV, indicating the weak bonding strength of H. Because the adjacent layers of Nb<sub>2</sub>S<sub>2</sub>C are coupled via weak vdW interactions, during the material synthesis, the number of layers can vary greatly. We, therefore, calculate the  $\Delta G_{H^*}$  for 10 unit-cell-thick slab ( $n = 10$ ) also to study the effect of slab thickness on the HER performance. At the same H coverage of 1, the  $\Delta G_{H^*}$  for  $n = 10$  is 1.097 eV, showing a negligible modification compared with that of  $n = 5$  ( $\Delta G_{H^*} = 1.10 \text{ eV}$ ). It confirms that the HER performance of the material is robust against the slab thickness. Besides, we also explore the possibility of obtaining monolayer (ML) Nb<sub>2</sub>S<sub>2</sub>C (see details in the Supporting Information) and calculate its  $\Delta G_{H^*}$ . It's noted that the structure of ML Nb<sub>2</sub>S<sub>2</sub>C

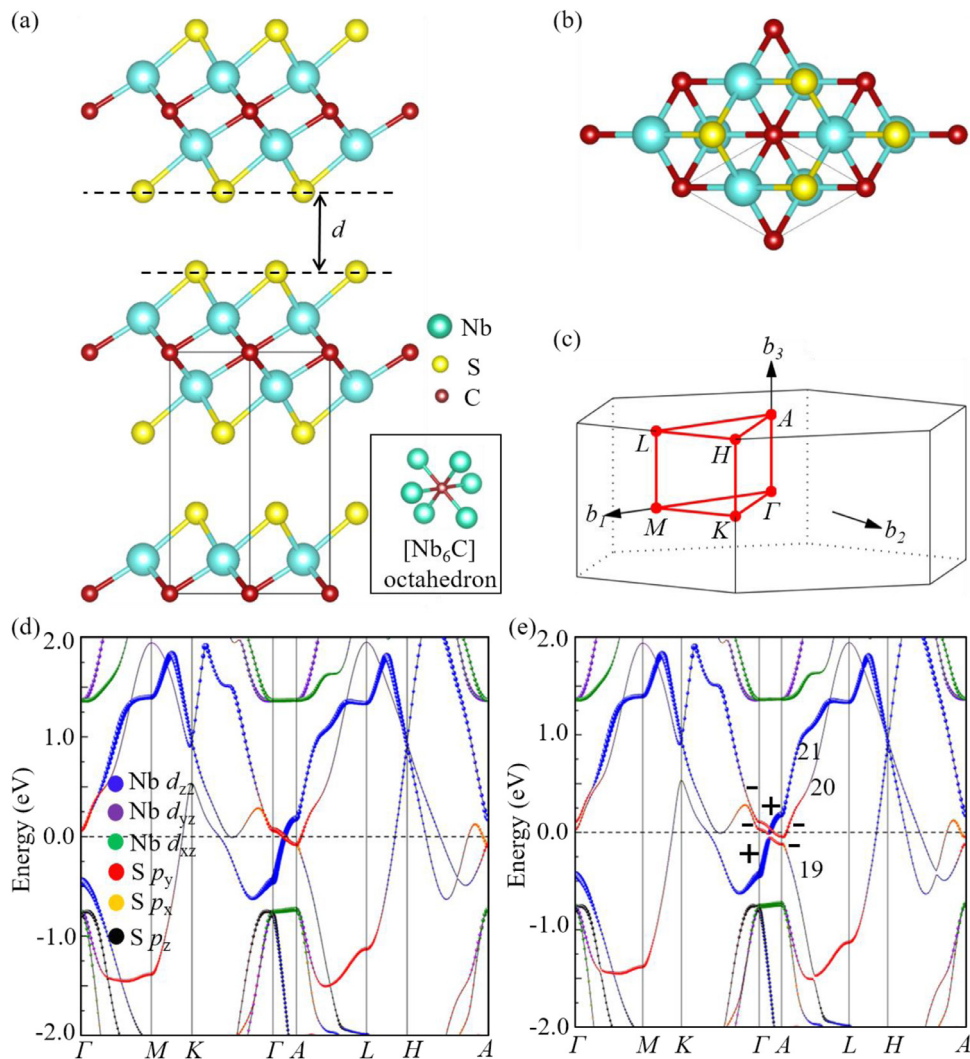
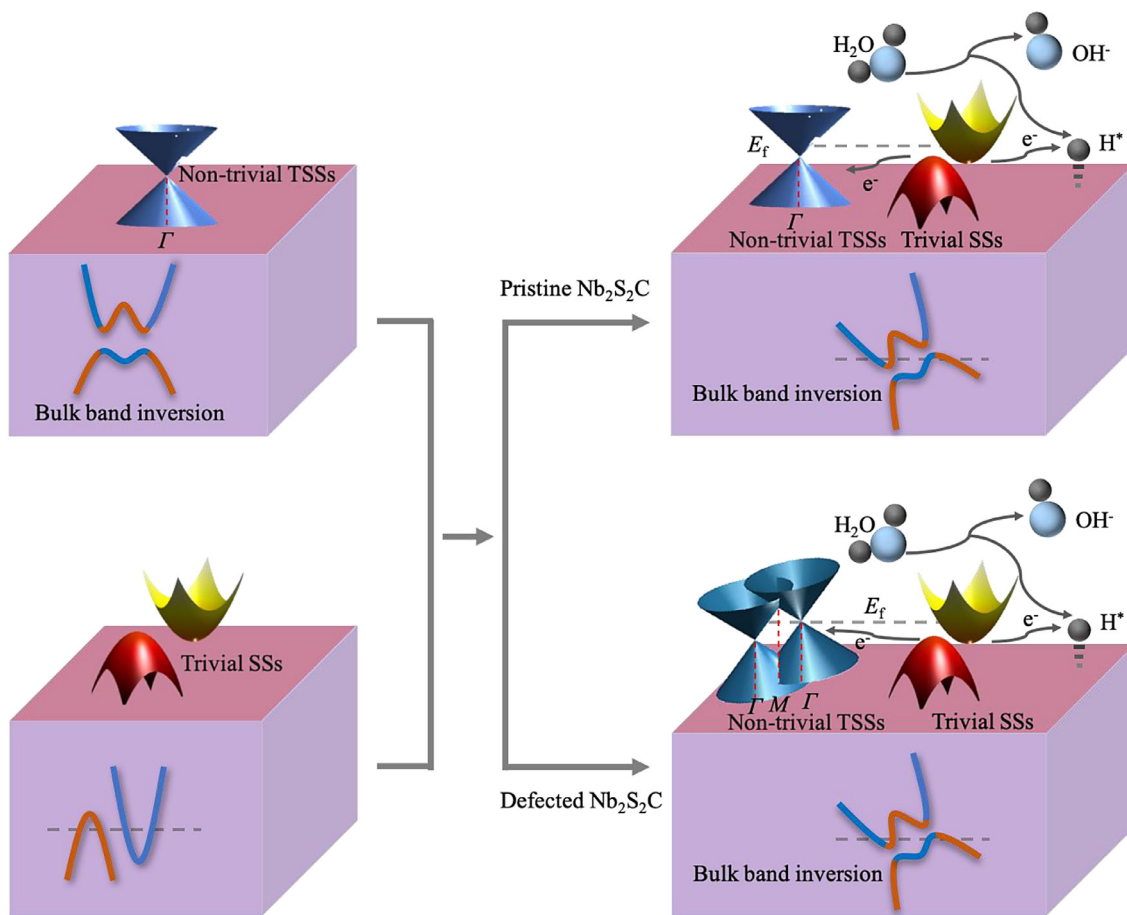


**Fig. 1.** (a) Side and (b) top view of the crystal structure of 1T-Nb<sub>2</sub>S<sub>2</sub>C. The interlayer distance *d* is 2.855 Å, which is the typical vdW distance. (c) Primitive Brillouin zone of Nb<sub>2</sub>S<sub>2</sub>C. Band structures of Nb<sub>2</sub>S<sub>2</sub>C (d) without and (e) with spin-orbital coupling. Band inversion occurred between the Nb-4*d*<sub>z2</sub>, S-3*p*<sub>x</sub>, and S-3*p*<sub>y</sub> orbitals in the vicinity of the  $\Gamma$  point. The parities of the double degenerate band numbers 19, 20, and 21 are illustrated.

is similar to that of MXenes [43], but quite different from the MXenes which are usually synthesized by selectively etching away the A-element atoms from parent layered ternary or quaternary carbides/nitrides in the solution of HF, giving rise to the mixture of O, OH and F functional groups presented on the basal planes, the ML Nb<sub>2</sub>S<sub>2</sub>C with ideal homogeneous surface S termination can be obtained by exfoliating from the bulk Nb<sub>2</sub>S<sub>2</sub>C crystal. Our results indicate that the ML Nb<sub>2</sub>S<sub>2</sub>C has low cleavage energy (0.42 J/m<sup>2</sup>) comparable to MoS<sub>2</sub>. Besides, it has high cohesive energy, excellent dynamic stability, and good thermal stability. Hence, it is possible to obtain ML Nb<sub>2</sub>S<sub>2</sub>C in the experiment. Based on our calculation, the  $\Delta G_{H^*}$  of ML Nb<sub>2</sub>S<sub>2</sub>C is 1.01 eV at the H coverage of ¼, much smaller than that of 2H-MoS<sub>2</sub>, which could be ascribed to the good conductivity presented in the ML Nb<sub>2</sub>S<sub>2</sub>C. Moreover, it's worth noting that under the same H coverage, the bulk and surface properties of Nb<sub>2</sub>S<sub>2</sub>C for H adsorption are superior to those of ML Nb<sub>2</sub>S<sub>2</sub>C and 2H-MoS<sub>2</sub>. It indicates that the bulk properties of Nb<sub>2</sub>S<sub>2</sub>C can benefit for the H adsorption, but only to a certain extent, because the binding strength toward the adsorption of H is still too weak.

Point defects are unavoidable during the material preparation processes. It has been widely recognized that the defects in MoS<sub>2</sub>

play an essential role in altering its properties in various ways, and hence, affect its performance [14–16]. Nb<sub>2</sub>S<sub>2</sub>C has MoS<sub>2</sub>-like S-terminated basal plane synthesized by the topo-chemical reaction. In addition, the presence of the TSSs is robust against the defects, impurities and disorders [25,27]. Those all motivate us to study the defective Nb<sub>2</sub>S<sub>2</sub>C basal plane. To explore the interaction mechanism for TSSs and trivial SSs effects on the HER activity, we consider a small concentration of S-vacancy on the Nb<sub>2</sub>S<sub>2</sub>C basal plane by creating one S vacancy on the 3 × 3 Nb<sub>2</sub>S<sub>2</sub>C basal plane. Based on the formation energy analysis, we find that it is possible to obtain ~11% S-vacancy on Nb<sub>2</sub>S<sub>2</sub>C. Besides, this S-vacancy site is expected to be preferentially occupied by H other than H<sub>2</sub>O molecule under the acidic aqueous conditions (see details in the Supporting Information). We find that the hollow site of three exposed Nb atom becomes the energetically most favorable site for H adsorption as shown in the inset of Fig. 2 and Figure S2 (b), and the  $\Delta G_{H^*}$  is greatly optimized to 0.31 eV. Due to the broken Nb-S bonds, it induces the formation of local dangling bonds, and therefore, we predict that the combined presence of trivial dangling-bond SSs and nontrivial TSSs facilitates the HER at the basal plane, where  $\Delta G_{H^*}$  is close to 0 eV.



**Scheme 1.** The synergistic effect between non-trivial topological and trivial surface states provide a new way for activating the basal plane electrocatalytic HER activity, and even for gaining insight into the catalytic mechanism.

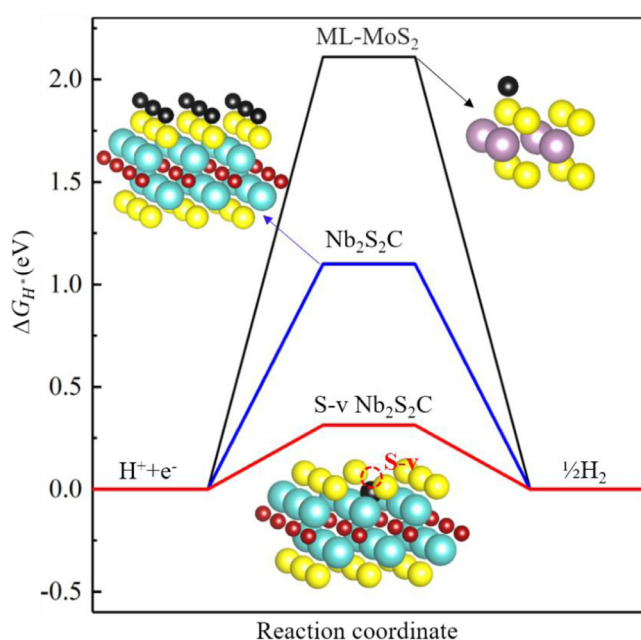


**Fig. 2.** Calculated Gibbs free energy of pristine  $\text{Nb}_2\text{S}_2\text{C}$  basal plane with H coverage of 1 and S-vacancy  $\text{Nb}_2\text{S}_2\text{C}$  basal plane (S-v  $\text{Nb}_2\text{S}_2\text{C}$ ). The Gibbs free energy of  $\text{ML-MoS}_2$  [44] is also included for comparison. The Gibbs free energy of  $\text{Nb}_2\text{S}_2\text{C}$  and S-v  $\text{Nb}_2\text{S}_2\text{C}$  with H atom (black ball) adsorbing on the basal plane. Herein, the thickness of the one-unit-cell is displayed for  $\text{Nb}_2\text{S}_2\text{C}$  and S-v  $\text{Nb}_2\text{S}_2\text{C}$ , while their five-unit-cell-thick slabs are used for the calculations.

### 3.3. Surface properties of pristine $\text{Nb}_2\text{S}_2\text{C}$ basal plane before and after H adsorption

The SSs play an important role in surface catalytic reactions. Both trivial SSs and nontrivial TSSs are present on the  $\text{Nb}_2\text{S}_2\text{C}$  basal plane, and their synergistic effects determine the adsorption, desorption, and all kinetic processes on the surface. Nevertheless, the relative magnitude of the effects depends on the specific system. However, compared with the local surface properties of the substrates, the effect of the global properties based on the TSSs on the catalytic activity is often neglected. To understand the mechanism behind the remarkable catalytic activity of  $\text{Nb}_2\text{S}_2\text{C}$ , we comprehensively study the surface properties of the  $\text{Nb}_2\text{S}_2\text{C}$  basal plane before and after H adsorption.

Owing to topological protection, the TSSs are robust but their shapes are strongly dependent on the details of the environments of the surfaces. As presented in Figs. 3(a) and S5 (a), for pristine  $\text{Nb}_2\text{S}_2\text{C}$  basal plane, before H adsorption, the Dirac points associated with the upper-surface TSSs emerge at approximately 0.2 eV below the Fermi level, and are mainly dominated by the S-3p<sub>x</sub> and S-3p<sub>y</sub> orbitals. Furthermore, the partial charge density distribution of the upper-surface TSSs at the  $\Gamma$  point presented in Fig. 3(c) indicates that the TSSs are located on the surface S atoms. Therefore, these findings strongly indicate that the TSSs are distributed on the basal plane, which plays an important role in surface catalytic reactions. Moreover, owing to the weak coupling between the  $\text{Nb}_2\text{S}_2\text{C}$  layers, after the creation of the  $\text{Nb}_2\text{S}_2\text{C}$  (001) surface, trivial SSs present on the surface. That is confirmed by the presence of some S-3p<sub>z</sub>-orbital-derived density of states near the Fermi level, as il-

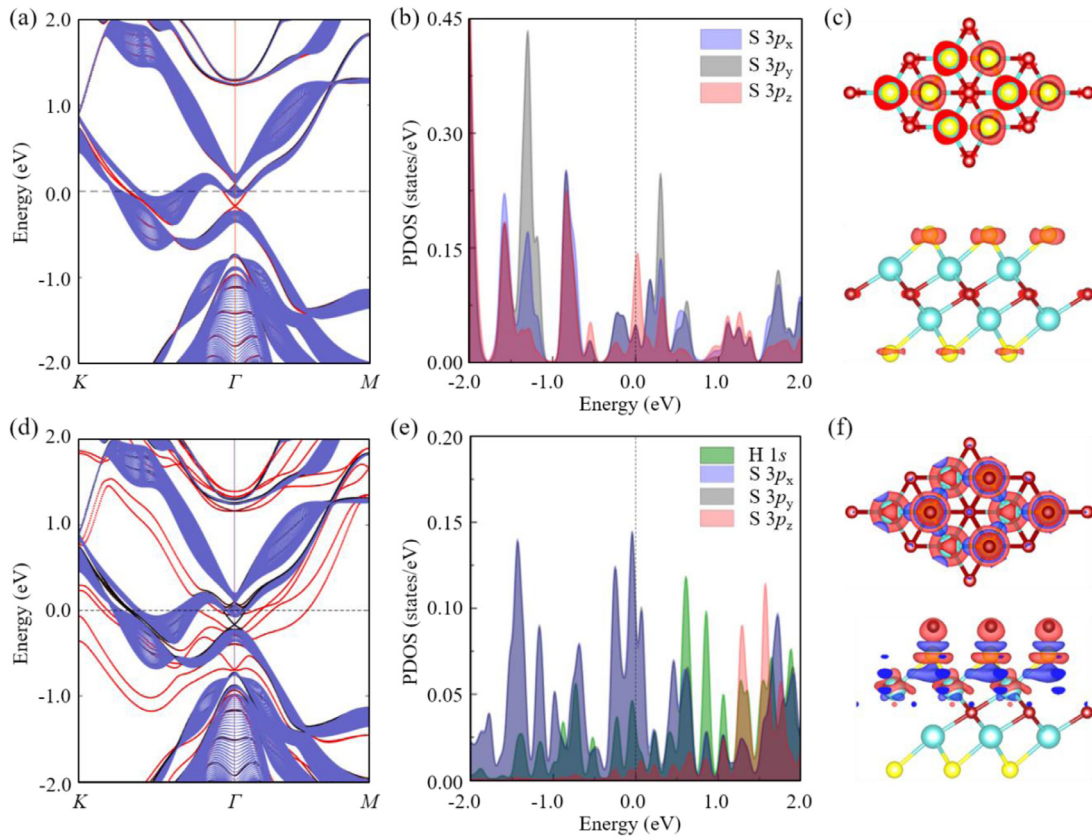


**Fig. 3.** Surface properties of the  $1 \times 1$  pristine  $\text{Nb}_2\text{S}_2\text{C}$  basal plane before and after H adsorption. Surface energy dispersion (a) before and (d) after H adsorption. The red lines indicate the surface states projected from the top one-unit-cell. The bulk projected states are shown in blue as the background. Projected density of states on the surface S atom (b) before and (e) after H adsorption. (c) Partial charge density distribution of pristine  $\text{Nb}_2\text{S}_2\text{C}$  at the  $\Gamma$  point within the energy range of  $-0.2$  to  $-0.1$  eV. (f) Charge density difference plot of H adsorbed on the  $\text{Nb}_2\text{S}_2\text{C}$  basal plane. The isosurface values are all set to  $0.005 \text{ e}/\text{\AA}^3$ . The thickness of the one-unit-cell is displayed in (c) and (f), and a five-unit-cell-thick slab is used for the calculations.

lustrated in Figs. 3(b) and S5 (a), suggesting the coexistence of the S-3p<sub>z</sub>-orbital-derived trivial SSs on the  $\text{Nb}_2\text{S}_2\text{C}$  basal plane.

After H adsorption, the chemically active S-3p orbitals can interact with the adsorbed H, the S-3p orbitals change significantly, the peak of the S-3p<sub>z</sub> orbitals at the Fermi level disappears, and empty S-3p<sub>z</sub> orbitals present in the energy range of  $1.2$ – $1.8$  eV, as demonstrated by the projected density of states in Fig. 3(e) and S-3p<sub>z</sub>-orbital-weighted band structure in Figure S5 (b). In addition, more occupied S-3p<sub>x</sub> and S-3p<sub>y</sub>-orbital-derived states emerge below the Fermi level after H adsorption, and orbital hybridization occurs between the H-1 s and S-3p orbitals in the energy range of  $0$ – $1.7$  eV. Moreover, as presented in Fig. 3(f), charges are redistributed; charge accumulation occurs on the adsorbed H atom and S-3p<sub>x</sub> and S-3p<sub>y</sub> orbitals, whereas charge is depleted on the S-3p<sub>z</sub> orbitals. Therefore, the trivial SSs and nontrivial TSSs are directly involved in H adsorption, and that is also confirmed by the orbital-weighted band structure diagrams in Figures S5 and S6.

#### 3.4. Surface properties of pristine $\text{Nb}_2\text{S}_2\text{C}$ and defected $\text{Nb}_2\text{S}_2\text{C}$ before and after H adsorption

After we confirm the crucial role of the synergistic effect of the trivial SSs and nontrivial TSSs during H adsorption, we conclude that the H binding strength on the basal plane of  $\text{Nb}_2\text{S}_2\text{C}$  is greatly improved compared with that on 2H-MoS<sub>2</sub>, which does not contain S-3p<sub>z</sub>-orbital-derived trivial SSs or nontrivial TSSs on its pristine S-terminated surface. However, the small fraction of trivial SSs and their delocalization caused by the S-3p<sub>z</sub> orbitals of the pristine  $\text{Nb}_2\text{S}_2\text{C}$  basal plane limit H binding and facilitate the weak inter-

actions between substrate and H. These findings are reflected in the relatively large  $\Delta G_{\text{H}*}$  of  $1.10$  eV and small fraction of charges ( $0.027 \text{ e}^-$ ) that transferred from the substrate to the adsorbed H.

With one S vacancy on the  $3 \times 3$   $\text{Nb}_2\text{S}_2\text{C}$  basal plane, the  $\Delta G_{\text{H}*}$  is greatly optimized to  $0.31$  eV. Before the creation of the S vacancy, as shown in Figs. 4(a)–(c) and S7 (a), we find that for the target Nb atom, it is the Nb-4d<sub>z<sub>2</sub></sub> orbitals that mainly dominate the upper-surface TSS Dirac bands. The Nb-4d<sub>z<sub>2</sub></sub> orbital is perpendicular to the basal plane and thus has a suitable orbital orientation for interacting with H 1 s orbital. However, it locates at the sublayer, which prevents overlap between the Nb-4d<sub>z<sub>2</sub></sub> with orbitals of the hydrogen adsorbates. When S-vacancy is introduced, this Nb atom is exposed, as shown in Figs. 4(d)–(f) and S7 (b), we find that the upper surface TSS Dirac bands are still mainly dominated by the Nb-4d<sub>z<sub>2</sub></sub> orbitals. Owing to inversion symmetry breaking, upper and bottom TSS Dirac bands are not degenerated anymore. With broken Nb-S bonds on the surface, new bands appear around  $-0.5$  eV below the Fermi level, and these states are mainly dominated by Nb-4d<sub>x<sub>2</sub></sub> and Nb-4d<sub>xz</sub> orbitals. The corresponding partial charge density distribution in Fig. 4(f) indicates that these new states mainly localize around the S-vacancy, and they are responsible for hydrogen adsorption on the S-vacancy. After H adsorption, as shown in Figs. 4(g)–(i), S2 (b), and S7 (c), the H atom prefers to stay at the hollow site of three exposed Nb atoms. Due to the suitable orbital orientation, the chemically active Nb-4d<sub>xz</sub>, Nb-4d<sub>x<sub>2</sub></sub>, and Nb-4d<sub>z<sub>2</sub></sub> states can interact strongly with the adsorbed H and hybridize strongly with the H-1 s orbitals. Besides, these states change significantly after H adsorption. The charge density differences and Bader charge analysis indicate that the charge accumu-

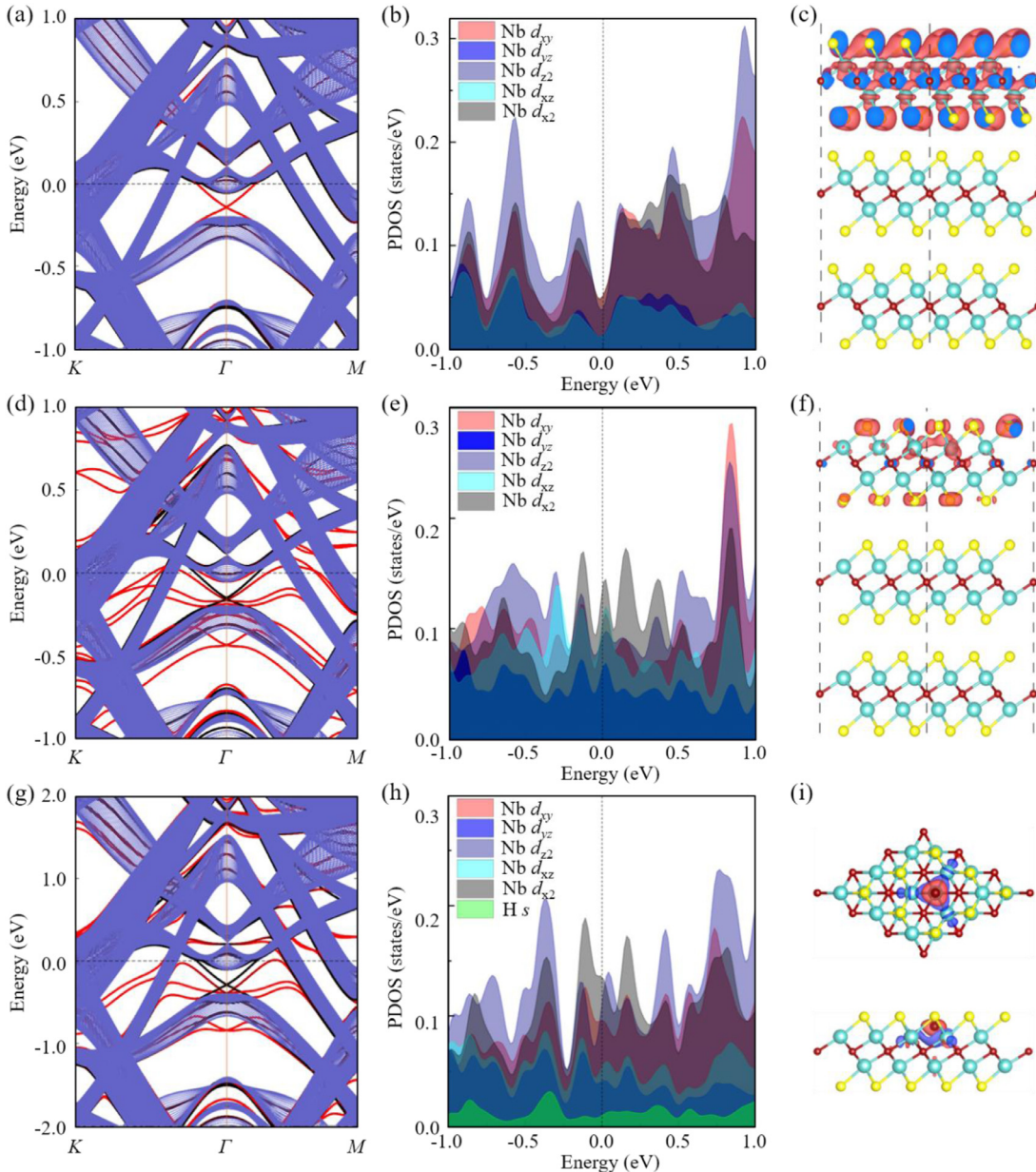


**Fig. 4.** Surface properties of  $3 \times 3$  pristine  $\text{Nb}_2\text{S}_2\text{C}$  and  $3 \times 3$   $\text{Nb}_2\text{S}_2\text{C}$  with one S vacancy before and after H adsorption. Surface energy dispersion of (a) pristine  $\text{Nb}_2\text{S}_2\text{C}$  and 11% S-vacancy  $\text{Nb}_2\text{S}_2\text{C}$  (d) before and (g) after H adsorption. The red lines indicate the surface states projected from the top one-unit-cell. The bulk projected states are shown in blue as the background. Projected density of states on the same Nb atom (as indicated by the red circle in Figure S2 (b)) for (b) pristine  $\text{Nb}_2\text{S}_2\text{C}$  and 11% S-vacancy  $\text{Nb}_2\text{S}_2\text{C}$  (e) before and (h) after H adsorption. (c) Partial charge density distribution of pristine  $\text{Nb}_2\text{S}_2\text{C}$  at the  $\Gamma$  point within the energy range of -0.2 to -0.1 eV. The isosurface value is set to  $5 \times 10^{-5} \text{ e}/\text{\AA}^3$ . (f) Partial charge density distribution of 11% S-vacancy  $\text{Nb}_2\text{S}_2\text{C}$  at the  $\Gamma$  point within the energy range of -0.45 to -0.35 eV. The isosurface value is set to  $4 \times 10^{-4} \text{ e}/\text{\AA}^3$ . (i) Charge density difference plot of H adsorbed on the 11% S-vacancy  $\text{Nb}_2\text{S}_2\text{C}$  basal plane. The isosurface value is set to  $0.002 \text{ e}/\text{\AA}^3$ . It's noted that the five-unit-cell-thick slabs are used for all calculations, while the thickness of the three-unit-cells is displayed in (c) and (f), and one-unit-cell is displayed in (i).

lation happens around the adsorbed H with s orbital shape, and overall, the H atom acquires a large number of charges of up to  $0.471 \text{ e}^-$  from the neighboring Nb atoms. Consequently, the H-1 s bands disperse in the deep energy region below the Fermi level, as illustrated in Figure S8. The elegant synergistic effect of the robust Nb- $4d_{z^2}$ -orbital-dominated TSSs and the Nb- $4d_{xz}$  and Nb- $4d_{x^2}$ -orbital-dominated dangling-bond SSs contribute to the greatly optimized Gibbs free energy for electrocatalytic hydrogen evolution.

It worth noting that normally, for topological trivial materials like  $\text{MoS}_2$ , by defect engineering, one can create dangling bonds SSs to enhance the adsorbate binding strength. In our work, by introducing the S-defect, we can expose the Nb atom on which the

TSSs located, therefore, we not only have the dangling bonds SSs due to the broken Nb-S bonds but also have the exposed TSSs that can participate in the chemical reaction that happens at the surfaces, they can cooperate with each other to modulate the adsorbate binding strength. The joint utilization of TSSs and dangling bonds SSs opens a new avenue toward activating the basal plane catalytic activity.

#### 4. Conclusions

In conclusion, we demonstrate a highly desirable new strategy for activating the inert basal plane by jointly utilizing the trivial dangling-bond SSs and TSSs of the  $\text{Nb}_2\text{S}_2\text{C}$  basal plane. Specifi-

cally, bulk  $\text{Nb}_2\text{S}_2\text{C}$  is a topological semimetal with the nontrivial  $Z_2$  index of (1; 0,0,1). Upon H adsorption, we determine that the upper-surface TSSs are directly involved in H binding and the TSSs for both the pristine and defective  $\text{Nb}_2\text{S}_2\text{C}$  change significantly. For pristine  $\text{Nb}_2\text{S}_2\text{C}$  basal plane, the S- $3p_x$  and S- $3p_y$ -orbital-dominated TSSs act as electron acceptors to modulate the binding strength between the substrate and H, while the S- $3p_z$ -orbital-dominated trivial SSs behave as the electron baths for H adsorption. It indicates the equally important contribution of trivial SSs and nontrivial TSSs for surface catalytic reactions. For defective  $\text{Nb}_2\text{S}_2\text{C}$ , it exposes the Nb atom on the basal plane and induces more local trivial SSs around Fermi level, hence, the chemically active Nb- $4d_{z^2}$ -orbital-dominated TSSs and Nb- $4d_{xz}$ ,  $4d_{x^2}$ -orbital-dominated trivial SSs can interact directly with the adsorbed H. Owing to the synergistic effect of trivial SSs and nontrivial TSSs, the defective  $\text{Nb}_2\text{S}_2\text{C}$  basal plane presents greatly optimized activity toward HER with a low  $|\Delta G_{H^*}|$  of 0.31 eV. This study provides a promising strategy for the optimization of the electrocatalytic hydrogen evolution activity on the basal-plane of  $\text{Nb}_2\text{S}_2\text{C}$  via the synergistic effect of trivial SSs and nontrivial TSSs.

## Author contributions

Qun Yang conceived the idea, designed the study, analyzed the data, performed all calculations, and wrote the manuscript. Congcong Le assisted with the theoretical analysis. Guowei Li gave scientific advice. Yan Sun and Thomas Heine modified the manuscript and gave scientific advice. The project was supervised by Claudia Felser. All authors discussed the results and commented on the manuscript.

## Declaration of competing interest

The authors declare no competing interests

## Acknowledgements

This work was financially supported by the European Research Council (ERC Advanced Grant No. 742068 'TOPMAT'). We also acknowledge funding by the DFG through SFB 1143 (project ID. 247310070) and the Würzburg-Dresden Cluster of Excellence on Complexity and Topology in Quantum Matter ct.qmat (EXC2147, project ID. 39085490) and via DFG project HE 3543/35-1. Some of our calculations are carried on the cluster of MPCDF, Max Planck society.

## Supplementary materials

Supplementary material associated with this article can be found, in the online version, at doi:10.1016/j.apmt.2020.100921.

## References

- [1] X. Wang, K. Maeda, A. Thomas, K. Takanabe, G. Xin, J.M. Carlsson, K. Domen, M. Antonietti, A metal-free polymeric photocatalyst for hydrogen production from water under visible light, *Nat. Mater.* 8 (2009) 76–80.
- [2] J.A.J.S. Turner, Sustainable hydrogen production, *Science* 305 (2004) 972–974.
- [3] J.K. Nørskov, T. Bligaard, A. Logadottir, J.R. Kitchin, J.G. Chen, S. Pandelov, U. Stimming, Trends in the exchange current for hydrogen evolution, *J. Electrochemical. Soc.* 152 (2005) J23–J26.
- [4] B. Hinnenmann, P.G. Moses, J. Bonde, K.P. Jørgensen, J.H. Nielsen, S. Horch, I. Chorkendorff, J.K. Nørskov, Biomimetic hydrogen evolution:  $\text{MoS}_2$  nanoparticles as catalyst for hydrogen evolution, *J. Am. Chem. Soc.* 127 (2005) 5308–5309.
- [5] H.I. Karunadasa, E. Montalvo, Y.J. Sun, M. Majda, J.R. Long, C.J. Chang, A molecular  $\text{MoS}_2$  edge site mimic for catalytic hydrogen generation, *Science* 335 (2012) 698–702.
- [6] J. Greeley, T.F. Jaramillo, J. Bonde, I.B. Chorkendorff, J.K. Nørskov, Computational high-throughput screening of electrocatalytic materials for hydrogen evolution, *Nat. Mater.* 5 (2006) 909–913.
- [7] Q. Ding, B. Song, P. Xu, S. Jin, Efficient electrocatalytic and photoelectrochemical hydrogen generation using  $\text{MoS}_2$  and related compounds, *Chem.* 1 (2016) 699–726.
- [8] X. Tian, D.S. Kim, S. Yang, C.J. Ciccarino, Y. Gong, Y. Yang, Y. Yang, B. Duschatko, Y. Yuan, P.M. Ajayan, Correlating the three-dimensional atomic defects and electronic properties of two-dimensional transition metal dichalcogenides, *Nat. Mater.* (2020) 1–7.
- [9] F. Ling, W. Kang, H. Jing, W. Zeng, Y. Chen, X. Liu, Y. Zhang, L. Qi, L. Fang, M. Zhou, Enhancing hydrogen evolution on the basal plane of transition metal dichalcogenide van der Waals heterostructures, *npj Comput. Mater.* 5 (2019) 1–7.
- [10] J. Kibsgaard, Z. Chen, B.N. Reinecke, T.F.J.N.m. Jaramillo, Engineering the surface structure of  $\text{MoS}_2$  to preferentially expose active edge sites for electrocatalysis, *Nat. Mater.* 11 (2012) 963.
- [11] T.F. Jaramillo, K.P. Jørgensen, J. Bonde, J.H. Nielsen, S. Horch, I. Chorkendorff, Identification of active edge sites for electrochemical  $\text{H}_2$  evolution from  $\text{MoS}_2$  nanocatalysts, *Science* 317 (2007) 100–102.
- [12] Q. Tang, D.E. Jiang, Mechanism of hydrogen evolution reaction on 1t- $\text{mos}_2$  from first principles, *Acs Catal.* 6 (2016) 4953–4961.
- [13] M.A. Lukowski, A.S. Daniel, F. Meng, A. Forticaux, L. Li, S. Jin, Enhanced hydrogen evolution catalysis from chemically exfoliated metallic  $\text{MoS}_2$  nanosheets, *J. Am. Chem. Soc.* 135 (2013) 10274–10277.
- [14] H. Li, C. Tsai, A.L. Koh, L. Cai, A.W. Contrryman, A.H. Fragapane, J. Zhao, H.S. Han, H.C. Manoharan, F. Abild-Pedersen, Activating and optimizing  $\text{MoS}_2$  basal planes for hydrogen evolution through the formation of strained sulphur vacancies, *Nat. Mater.* 15 (2016) 48–53.
- [15] Y. Chen, S. Huang, X. Ji, K. Adeppali, K. Yin, X. Ling, X. Wang, J. Xue, M. Dresselhaus, J. Kong, Tuning electronic structure of single layer  $\text{MoS}_2$  through defect and interface engineering, *ACS Nano* 12 (2018) 2569–2579.
- [16] W. Qiao, W. Xu, X. Xu, L. Wu, S. Yan, D. Wang, Construction of active orbital via single-atom cobalt anchoring on the surface of 1T- $\text{MoS}_2$  basal plane toward efficient hydrogen evolution, *ACS Appl. Energy Mater.* 3 (2020) 2315–2322.
- [17] S. Lu, W. Wang, S. Yang, W. Chen, Z. Zhuang, W. Tang, C. He, J. Qian, D. Ma, Y. Yang, Amorphous  $\text{MoS}_2$  confined in nitrogen-doped porous carbon for improved electrocatalytic stability toward hydrogen evolution reaction, *Nano Res.* 12 (2019) 3116–3122.
- [18] S. Geng, Y. Liu, Y.S. Yu, W. Yang, H. Li, Engineering defects and adjusting electronic structure on S doped  $\text{MoO}_2$  nanosheets toward highly active hydrogen evolution reaction, *Nano Res.* 13 (2020) 121–126.
- [19] H. Li, C. Tsai, A.L. Koh, L. Cai, A.W. Contrryman, A.H. Fragapane, J. Zhao, H.S. Han, H.C. Manoharan, F.J.N.m. Abild-Pedersen, Activating and optimizing  $\text{MoS}_2$  basal planes for hydrogen evolution through the formation of strained sulphur vacancies, *Nat. Mater.* 15 (2016) 48–53.
- [20] W. Wu, C. Niu, C. Wei, Y. Jia, C. Li, Q. Xu, Activation of  $\text{MoS}_2$  basal planes for hydrogen evolution by zinc, *Angew. Chem. Int. Ed. Engl.* 58 (2019) 2029–2033.
- [21] J. Deng, H. Li, J. Xiao, Y. Tu, D. Deng, H. Yang, H. Tian, J. Li, P. Ren, X.J.E. Bao, E. Science, Triggering the electrocatalytic hydrogen evolution activity of the inert two-dimensional  $\text{MoS}_2$  surface via single-atom metal doping, *Energy Environ. Sci.* 8 (2015) 1594–1601.
- [22] J.P. Xiao, L.Z. Kou, C.Y. Yam, T. Frauenheim, B.H. Yan, Toward rational design of catalysts supported on a topological insulator substrate, *Acs Catal.* 5 (2015) 7063–7067.
- [23] H. Chen, W. Zhu, D. Xiao, Z. Zhang, CO oxidation facilitated by robust surface states on Au-covered topological insulators, *Phys. Rev. Lett.* 107 (2011) 056804.
- [24] C.R. Rajamathi, U. Gupta, N. Kumar, H. Yang, Y. Sun, V. Suss, C. Shekhar, M. Schmidt, H. Blumtritt, P. Werner, B. Yan, S. Parkin, C. Felser, C.N.R. Rao, Weyl semimetals as hydrogen evolution catalysts, *Adv. Mater.* 29 (2017) 1606202.
- [25] L.Q. Li, J. Zeng, W. Qin, P. Cui, Z.Y. Zhang, Tuning the hydrogen activation reactivity on topological insulator heterostructures, *Nano Energy* 58 (2019) 40–46.
- [26] G. Li, Q. Xu, W. Shi, C. Fu, L. Jiao, M.E. Kamminga, M. Yu, H. Tuysuz, N. Kumar, V. Suss, R. Saha, A.K. Srivastava, S. Wirth, G. Auffermann, J. Gooth, S. Parkin, Y. Sun, E. Liu, C. Felser, Surface states in bulk single crystal of topological semimetal  $\text{Co}_3\text{Sn}_2\text{S}_2$  toward water oxidation, *Sci. Adv.* 5 (2019) eaaw9867.
- [27] Q. Yang, G. Li, K. Manna, F. Fan, C. Felser, Y. Sun, Topological engineering of Pt-group-metal-based chiral crystals toward high-efficiency hydrogen evolution catalysts, *Adv. Mater.* 32 (2020) 1908518.
- [28] J. Li, H. Ma, Q. Xie, S. Feng, S. Ullah, R. Li, J. Dong, D. Li, Y. Li, X.-Q. Chen, Topological quantum catalyst: dirac nodal line states and a potential electrocatalyst of hydrogen evolution in the TiSi family, *Sci. China Mater.* 61 (2018) 23–29.
- [29] Q. Xu, G. Li, Y. Zhang, Q. Yang, Y. Sun, C. Felser, Descriptor for hydrogen evolution catalysts based on the bulk band structure effect, *ACS Catal.* 10 (2020) 5042–5048.
- [30] G. Kresse, J. Furthmüller, Efficiency of ab-initio total energy calculations for metals and semiconductors using a plane-wave basis set, *Comput. Mater. Sci.* 6 (1996) 15–50.
- [31] G. Kresse, J. Furthmüller, Efficient iterative schemes for ab initio total-energy calculations using a plane-wave basis set, *Phys. Rev. B* 54 (1996) 11169.
- [32] G. Kresse, D. Joubert, From ultrasoft pseudopotentials to the projector augmented-wave method, *Phys. Rev. B* 59 (1999) 1758.
- [33] J.P. Perdew, K. Burke, M. Ernzerhof, Generalized gradient approximation made simple, *Phys. Rev. Lett.* 77 (1996) 3865.
- [34] S. Grimme, J. Antony, S. Ehrlich, H. Krieg, A consistent and accurate ab initio parametrization of density functional dispersion correction (DFT-D) for the 94 elements H–Pu, *J. Chem. Phys.* 132 (2010) 154104.

- [35] A.A. Mostofi, J.R. Yates, Y.S. Lee, I. Souza, D. Vanderbilt, N. Marzari, wannier90: a tool for obtaining maximally-localised Wannier functions, *Comput Phys Commun* 178 (2008) 685–699.
- [36] H.M. Weng, X. Dai, Z. Fang, Exploration and prediction of topological electronic materials based on first-principles calculations, *Mrs Bull.* 39 (2014) 849–858.
- [37] K. Sakamaki, H. Wada, H. Nozaki, Y. Onuki, M. Kawai, Topochemical formation of van der Waals type niobium carbosulfide 1T-Nb<sub>2</sub>S<sub>2</sub>C, *J. Alloy Compd.* 339 (2002) 283–292.
- [38] L. Fu, C.L. Kane, E.J. Mele, Topological insulators in three dimensions, *Phys. Rev. Lett.* 98 (2007) 106803.
- [39] B. Bradlyn, L. Elcoro, J. Cano, M. Vergniory, Z. Wang, C. Felser, M. Arroyo, B.A. Bernevig, Topological quantum chemistry, *Nature* 547 (2017) 298–305.
- [40] M. Vergniory, L. Elcoro, C. Felser, N. Regnault, B.A. Bernevig, Z. Wang, A complete catalogue of high-quality topological materials, *Nature* 566 (2019) 480–485.
- [41] T. Zhang, Y. Jiang, Z. Song, H. Huang, Y. He, Z. Fang, H. Weng, C. Fang, Catalogue of topological electronic materials, *Nature* 566 (2019) 475–479.
- [42] K. Mathew, R. Sundararaman, K. Letchworth-Weaver, T. Arias, R.G. Hennig, Implicit solvation model for density-functional study of nanocrystal surfaces and reaction pathways, *J. Chem. Phys.* 140 (2014) 084106.
- [43] Y. Gogotsi, B. Anasori, in: *The Rise of MXenes*, ACS Publications, 2019, pp. 8491–8494. ACS Nano.
- [44] R. Li, L. Yang, T. Xiong, Y. Wu, L. Cao, D. Yuan, W. Zhou, Nitrogen doped MoS<sub>2</sub> nanosheets synthesized via a low-temperature process as electrocatalysts with enhanced activity for hydrogen evolution reaction, *J. Power Sources* 356 (2017) 133–139.